HHS Public Access

Author manuscript

J Mol Biol. Author manuscript; available in PMC 2020 June 30.

Published in final edited form as:

J Mol Biol. 2020 February 14; 432(4): 991–1007. doi:10.1016/j.jmb.2019.12.010.

Ribosomal Protein L11 Selectively Stabilizes a Tertiary Structure of the GTPase Center rRNA Domain

Robb Welty[1,5], **Michael Rau**[1], **Suzette Pabit**[2], **Mark S. Dunstan**[3], **Graeme L. Conn**[4], **Lois Pollack**[2], **Kathleen B. Hall**[1]

[1]-Department of Biochemistry and Molecular Biophysics, Washington University School of Medicine, 660 S Euclid Ave, St Louis, MO, 63110, USA

[2]-School of Applied and Engineering Physics, Cornell University, Clark Hall, Ithaca, NY, 14853, USA

[3]-Manchester Institute of Biotechnology, University of Manchester, 131 Princess Street, Manchester, M1 7DN, United Kingdom

[4]-Department of Biochemistry, Emory University School of Medicine, 1510 Clifton Road, Atlanta GA, 30322, USA

[5]-Department of Chemistry, University of Michigan, Ann Arbor, MI, 48109, USA

Abstract

The GTPase Center (GAC) RNA domain in bacterial 23S rRNA is directly bound by ribosomal protein L11, and this complex is essential to ribosome function. Previous cocrystal structures of the 58-nucleotide GAC RNA bound to L11 revealed the intricate tertiary fold of the RNA domain, with one monovalent and several divalent ions located in specific sites within the structure. Here, we report a new crystal structure of the free GAC that is essentially identical to the L11-bound structure, which retains many common sites of divalent ion occupation. This new structure demonstrates that RNA alone folds into its tertiary structure with bound divalent ions. In solution, we find that this tertiary structure is not static, but rather is best described as an ensemble of states. While L11 protein cannot bind to the GAC until the RNA has adopted its tertiary structure, new experimental data show that L11 binds to Mg^{2+}-dependent folded states, which we suggest lie along the folding pathway of the RNA. We propose that L11 stabilizes a specific GAC RNA tertiary state, corresponding to the crystal structure, and that this structure reflects the functionally critical conformation of the rRNA domain in the fully assembled ribosome.

Keywords

L11 stalk; RNA folding; GTPase center; protein:RNA complex; RNA crystal structure

Correspondence to Kathleen B. Hall: Department of Biochemistry and Molecular Biophysics, CB 8231, Washington University School of Medicine, 660 S Euclid Ave, St Louis, MO, 63110, USA. kathleenhal@gmail.com.

Author Contribution

Robb Welty: conceptualization, methodology, software, investigation, writing. **Suzette Pabit**: conceptualization, investigation, analysis, writing. **Michael Rau**: investigation, resources. **Mark Dunstan**: investigation, analysis; **Graeme Conn**: formal analysis, writing, conceptualization. **Lois Pollack**: conceptualization, analysis, writing; **Kathleen Hall**: conceptualization, writing, investigation, supervision, administration.

Introduction

The 58-nucleotide GTPase center (GAC; nt 1051–1108, *E. coli* numbering) ribosomal RNA (rRNA) domain is essential for translation initiation, elongation and release, interacting with aminoacyl-tRNA/EF-Tu [1,2], EF-G [1,3,4], and release factor 2 (RF2) [5] during these steps in protein synthesis. As such, the GAC RNA is among the most highly conserved rRNA sequences in 23S/28S rRNA [6]. The prokaryotic L11 ribosomal protein (rpL12 in eukaryotes) binds directly to the GAC [2,7–11], and it too makes contact with ribosomal cofactors. Consistent with these critical roles in the three main steps of translation, the GAC/L11 complex (also called the L11 stalk or L11 arm) is conserved in all organisms.

The key contributions of the GAC RNA and L11 to translation have motivated numerous *in vivo* functional studies as well as many biochemical and structural investigations of their interactions. Conservation of both RNA and protein is exemplified by retained binding of *E. coli* L11 to the GAC RNAs from *S. cerevisiae* and mouse [12] and the observation that *in vivo* swapping of the *E. coli* GAC with that of *S cerevisiae* (and *vice versa*) had no apparent effect on cell growth [13]. While *E. coli* L11 can be deleted (with only a resultant slow growth phenotype), it is lethal to delete the entire 58-nt GAC RNA domain [14]. Deleting a hairpin loop of GAC is also dominant-lethal, although these ribosomes are active *in vitro* [14], and even some single mutations in GAC can be lethal [15,16]. Thus, the critical nature of these 58 nucleotides for protein synthesis in all organisms warrants further detailed investigation of GAC RNA-L11 association.

The GAC domain adopts an intricate tertiary structure. In solution, thermodynamic studies of GAC folding showed that, in a background of KCl, divalent ions were necessary to stabilize the tertiary structure [17–20]. In our previous kinetic studies of Mg^{2+}-dependent GAC tertiary folding, we found that the transition from secondary structure to tertiary structure has four intermediate states [21]. Our kinetic scheme for GAC folding includes two steps of divalent ion binding within the first 100 ms. Slower transitions, with rates from seconds to tens of seconds, subsequently produce the folded tertiary structures. We concluded from our previous studies that, in solution, the free GAC RNA tertiary structure is really an ensemble of conformations.

L11 has two structural domains connected by a flexible linker. In structural studies using SANS [22] and NMR [10] of the full-length L11 complex with RNA, the N-terminal domain (NTD) appears very dynamic; it bends and rotates when RNA is present. However, additional shifts in 1D-NMR spectra that appear when RNA is complexed with full-length L11 [10] point to at least some limited interactions between the NTD and RNA. In contrast, the 76-residue C-terminal domain (CTD) directly binds to the GAC, leading to the extensive interactions with the RNA in cocrystal structures [23,24] (Fig. 1). As a result, the isolated CTD of L11 has historically been used for *in vitro* binding experiments [11,25–29] and the individual domain is used throughout this work. The *E. coli* L11 CTD has modest thermodynamic stability *in vitro* [11], so most experiments used the analogous construct from *B. stearothermophilus* or *Thermus thermophilus*. These L11 CTDs bind *E. coli* GAC with nanomolar affinity under conditions where the RNA has folded into its tertiary structure [27,30]. Despite phylogenetic variations of protein and RNA, crystal structures of this

complex are virtually identical whether determined as an isolated binary system [23,24] or as a component of the large ribosomal subunit or assembled ribosome [3,31,32].

Since the folded GAC RNA is not a single structure in solution, even in the presence of Mg^{2+} and K^{+} ions, we have revisited the binding mechanism of L11. Specifically, we wanted to understand at what point in the GAC folding path was the protein able to associate and then if it could influence the conformational state(s) of the RNA. First, we determined the crystal structure of the L11 protein-free RNA, to ask if it can adopt a structure similar to that observed in cocrystals. Then we used a combination of stopped-flow fluorescence, SAXS, NMR, and ITC, to examine when and how the L11 CTD was able to bind the GAC RNA. We concluded that L11 can only bind to GAC after the RNA has bound Mg^{2+}. In doing so, L11 binding alters the GAC RNA conformational ensemble to favor its fully folded tertiary state. Further, GAC conformational sampling is reduced when L11 is bound, which we propose is necessary in the context of the ribosome to optimally present its nucleotides for functionally essential interactions with ribosomal cofactors. Collectively, our findings provide a new appreciation for the role of L11 in maintaining the structure and stability of the GAC RNA and its role during protein synthesis.

Results

We needed to use several complementary methods to dissect the global and local responses of the GAC RNA to L11 CTD binding within our kinetic framework for GAC tertiary folding [21]. First, to determine the GAC tertiary fold in the absence of protein, we crystallized and determined the structure of the *E. coli* 58 nt domain. Next, to probe the Mg^{2+}-dependence of formation of specific GAC tertiary interactions, we used NMR with selectively ^{15}N-labeled GAC RNA with and without *T. thermophilus* (*Tth*) L11 CTD. To compare GAC folding kinetics in the presence and absence of *B. stearothermophilus (Bst)* L11 CTD, we monitored tertiary structure formation in stopped-flow fluorescence experiments with site-specific 2-aminopurine labeled GAC RNA. Steady-state fluorescence and SAXS allowed probing of the response of the folded RNA to the presence of *Bst* L11 CTD. We used the *E. coli* GAC U1061A mutant for all experiments with L11 CTDs, since it adopts a more stable tertiary structure than the wild-type sequence [33]. Data from the Draper lab has shown that both L11 CTDs bind with nanomolar affinity to this GAC when it is folded [27].

Crystal structure of the free 58 nt GAC RNA

Our previous kinetics experiments had indicated that the folded GAC RNA alone was best described as an ensemble of conformations, which depended on the Mg^{2+} concentration. In contrast, cocrystal structures with L11 constructs all showed a single GAC RNA structure. This structure has been assumed to represent the structure of the GAC RNA alone in solution, in the absence of other data. However, to most accurately interpret our RNA folding data and to understand how the L11:GAC RNA complex is formed, we needed to know if the protein-free GAC RNA could indeed adopt a similar structure.

To address this question, the crystal structure of the L11-free *E. coli* GAC RNA was determined at 2.72 Å resolution by molecular replacement using the structure of L11-CTD-bound GAC (**PDB ID 1HC8**) as a starting model. All water molecules, ions, and L11 were removed prior to molecular replacement and water and ions were manually built back into the structure after an initial round of refinement. The crystal asymmetric unit contains four copies of the GAC with clear, continuous electron density for all nucleotides in two chains (A and C) and reasonable density for Chain B. In contrast, significantly weaker, broken density was observed for chain D, which makes more limited contacts within the crystal, resulting in a model of poorer overall fit to the electron density. As a result, the descriptions of GAC RNA structure and RN-ion interactions that follow will focus only on chains A-C. After completing refinement, the final model of the free GAC RNA exhibits good overall geometry and has R_{work}/R_{free} of 20.4/26.0. Completedata collection and refinement statistics are presented in Table 1. The structures of all three copies of free GAC RNA (chains AeC) are essentially identical to each other and to the protein-bound state of the RNA (Fig. 2), with average all-atom RMSDs of 0.45, 0.40, and 0.54 Å for alignment of all free, all protein-bound, and protein-free/protein-bound GAC RNA structures, respectively.

Numerous ions were identified in the electron density maps for the free GAC, as expected (Fig. 3A). The total number of ions varied between the modeled RNA chains with the most identified for chains A and C, which exhibited overall higher quality maps. At the relatively modest resolution of the current structure, it is not possible to unambiguously identify ions based solely on electron density. However, correct identification can be accomplished by consideration of ions distances (e.g., ~2.0–2.2 Å for direct coordination of Mg^{2+}: for K^+, 2.7–3.5 Å) and geometry. The ions identified in the new structure fulfill these requirements and are therefore assigned with confidence. Three Mg^{2+} and one K^+ were found in all three chains, while two additional sites were identified in at least two copies of the RNA (Fig. 3A). These common K^+ and Mg^{2+} ion binding sites were also previously observed in the L11-CTD-bound GAC RNA structure [24]. Two ions modeled as Mg^{2+} in all three RNA chains involve inner sphere coordination. These ions bridge two regions of the GAC RNA brought into close proximity by the RNA tertiary fold and stabilize the unusual conformation of L43 (Fig. 3B and C). This new crystal structure demonstrates that the GAC alone, in the presence of K^+ and Mg^{2+}, can indeed adopt the single tertiary structure observed in cocrystals with L11 proteins. Since GAC RNA structures are virtually identical in all crystal structures, we consider this to be the dominant folded state of this RNA, including in solution when the ions are present.

The GAC-L11 complex at equilibrium

Binding

Binding of both *Tth* and *Bst* L11 CTDs to *E. coli* U1061A GAC was extensively studied as a function of salt and divalent ions by the Draper lab [28,34]. Using nitrocellulose filter binding, they observed that those CTDs were not capable of binding GAC RNA when it had only secondary structure. Their extensive investigation of the salt dependence of *Bst* L11 CTD binding measured K_D = 17 nM in 175 mM KCl, 3 mM $MgCl_2$, pH 7, and revealed that

pH and salt concentrations are sensitive determinants of binding affinity for this complex [28].

We used nitrocellulose filter binding experiments to measure binding affinities in solution conditions that we used for other experiments, as a control for protein activity and affinity (Fig. 4). For example, we measured affinity in 100 mM KCl ± 8 mM $MgCl_2$, and 300 mM KCl, 8 mM $MgCl_2$, 10 mM sodium cacodylate, pH 6.5. We used low salt (100 mM K^+) to favor any association that could occur in the absence of Mg^{2+}, but we saw no retention of the RNA:L11 complex until > μM protein, which we attribute to nonspecific sticking of the protein to the filter. In contrast, binding is so tight in 100 mM K^+, 8 mM Mg^{2+} that it is impossible to accurately measure the affinity. Other filter binding experiments for *Tth* L11 CTD binding to GAC U1061A in 10 mM sodium cacodylate pH 6.5, 5 mM $MgCl_2$, 175 mM KCl, gave K_D = 3.8 ± 0.7 nM, while K_D = 0.1 nM was determined for *Bst* L11 CTD binding in 350 mM KCl, 5 mM Mg^{2+}. These solution conditions bracket those used in NMR, SAXS, ITC, and fluorescence and thus indicate when complex formation will be stable.

Using isothermal titration calorimetry (ITC), we hoped to observe weak binding of *Tth* CTD to the GAC RNA secondary structure (in the absence of Mg^{2+}), which we could not detect by nitrocellulose filter binding. We reasoned that if the tertiary folded state of the RNA was among the ensemble of structures in solution in the absence of Mg^{2+}, then we might be able to detect binding by ITC as it is a true equilibrium approach, which exploits a distinct binding signal (changes in heat upon binding). Also, ITC provides direct determination of the binding enthalpy, which gives more insight into the thermodynamic driving mechanism.

ITC experiments were carried out in low salt to favor detection of weak binding by the *Tth* L11 CTD. In the absence of Mg^{2+}, the experiment shows evidence of weak association of L11 CTD with the GAC RNA. If we assume a 1:1 stoichiometry, we can fit the isotherm with K_D = 9 μM, suggesting that there is potentially some very weak binding. However, since the unconstrained fit gives a calculated n = 2.7, we have limited confidence in the accuracy.

In contrast, in 100 mM KCl in the presence of 3 mM Mg^{2+}, binding was stoichiometric (as expected; n = 1.16), with a distinct isotherm. The enthalpic contribution to L11 CTD binding ΔH = −7.4 kcal/mol, and we calculate ΔG = −10 kcal/mol, and ΔS = −59 cal/K-M. Fitting the data to a standard isotherm gives K_D = ~40 nM. This value differs 10× from measured binding by nitrocellulose filter binding, which likely reflects the exquisite sensitivity of this complex to the Mg^{2+} ion concentration [28]. We have now shown that in these conditions, binding is enthalpically driven and entropically unfavorable.

SAXS

To examine the global parameters of the RNA ensembles when bound by L11, we utilized small-angle X-ray scattering (SAXS). We previously found [21] that the scattering properties of the GAC RNA are sensitive to ion-induced folding: the GAC secondary structure has a calculated radius of gyration (*Rg*) of ~25 Å, while its folded tertiary structure has *Rg* = 21.3 ± 0.5 Å in the presence of Mg^{2+}. Now we compare the dimensions of the GAC RNA when L11 CTD is bound, to measure what effect, if any, the protein has on the

compaction of the RNA or the conformational ensemble. For example, in the absence of divalent ion, the protein might induce a compaction of the GAC RNA. Conversely, addition of protein to the compacted GAC tertiary structure could lead to further compaction or even an expansion. Therefore, we measured the steady-state SAXS scattering profiles of the GAC RNA with *Bst* L11 CTD in 100 mM KCl with and without added Mg^{2+}.

The plots of scattering intensity [I(q) vs q($Å^{-1}$)] and corresponding Kratky plots [I(q)*q^2 vs q] (Fig. 5) show the differential responses of the GAC RNA ± Mg^{2+}. The scattering vector q ($q = (4\pi/\lambda)\sin\theta$) is a function of the X-ray wavelength λ and the scattering angle 2θ. It is clear that addition of Mg^{2+} alters the GAC SAXS profile. A bell-shaped curve in the Kratky plot, with a peak at mid q, indicates a folded globular structure, whereas a broad profile with a plateau is typical of an extended structure [35]. Here, we see that in the absence of Mg^{2+}, the GAC RNA resembles an extended structure, but when Mg^{2+} is present, its global structure would be characterized as compacted.

We observed that the presence of the L11 CTD did not measurably alter the GAC RNA global dimensions. In Fig. 5A, the relative intensities of the SAXS profiles show that the protein has a much lower signal compared to the RNA and RNA with protein. When the protein was added to the GAC RNA in the absence of Mg^{2+}, there was no change in the RNA scattering profile (see normalized intensities, Fig. 5B). Since there is no significant increase in the scattering signal of the CTD L11 + RNA in KCl within dilution error, we conclude that in KCl only, L11 binding either 1) is transient and not detectable, or 2) does not occur at these concentrations (20 μM RNA/30 μM Protein), or 3) does not alter *Rg* of the GAC RNA.

The relative intensity increase seen when L11 CTD binds to the folded GAC RNA with Mg^{2+} suggests tight binding of RNA to protein (Fig. 5A). However, binding does not alter the intrinsic shape of the scattering profile of the RNA (Fig. 5B) when compared to the RNA in $MgCl_2$. The calculated *Rg* of folded GAC RNA in $MgCl_2$ with and without L11 CTD is indistinguishable within error, 21.3 ± 0.5 Å and 21.7 ± 0.4 Å, respectively. However, there is a small shift observed in the Kratky plot (Fig. 5C), consistent with a more compact structure. We interpret the SAXS data as showing that L11 CTD does not bind to GAC RNA secondary structure in these conditions, and when it does bind to the Mg^{2+}-dependent folded GAC, it does not significantly alter the RNA global structure.

2-Aminopurine fluorescence reports on L11 binding

Although SAXS data did not reveal a significant change in the global parameters of GAC RNA when L11 CTD bound, it is possible that there are local responses of the nucleotides to the bound protein. To probe for such responses, we used the fluorescent nucleobase 2-aminopurine (2AP) to report on local and global environments within the RNA. Five adenines within the GAC RNA were selected for substitution with 2AP, based on the GAC RNA-L11 CTD cocrystal structure [24], which do not hydrogen bond with other nucleotides in the RNA (to avoid disrupting an intramolecular contact). Each construct contained a single A-to-2AP substitution and, as we reported [36], they all adopted the tertiary structure. Further, the GAC RNA-L11 CTD cocrystal structure indicated that none of the five 2AP bases should make direct contact with L11 CTD (Fig. 6A and B).

Here, we use these five 2AP-GAC constructs in binding experiments to *Bst* L11 CTD to determine if the protein perturbs the fluorescence at each site. A change in 2AP fluorescence would suggest a change in the physical/chemical environment of the 2AP, as indeed we observe fluorescence changes in the transition from secondary structure to tertiary structure upon addition of Mg^{2+} (Fig. 6C). 2AP located at positions 1067 and 1069 exhibits large decreases in fluorescence intensity upon GAC folding (60 and 80%, respectively), consistent with a conformational change of the 1065–1073 loop as its nucleobases form base triples with H44. A substantial fluorescence increase of 2AP fluorescence at 1061 (35%) is consistent with loss of stacking interactions in the secondary structure as the nucleobase moves out of the duplex and stacks with A1070. 2AP1070 suffers a small (~5%) loss of fluorescence intensity upon folding. 2AP1095, in the U-turn of L44, has a (25%) fluorescence increase when the GAC folds, consistent with reduction of stacking. These substantial changes in fluorescence intensity can be directly related to conformational rearrangements in the transition from secondary structure to tertiary structure.

A change in the structure of the GAC when protein is bound could also lead to changes in 2AP fluorescence. When *Bst* L11 CTD is added to folded GAC RNA, we observe that the fluorescence intensity at each 2AP site does respond to protein binding. However, the changes in fluorescence intensity are very modest, and with the exception of position 1070 (and less striking 1095), they follow the trend due to the secondary→tertiary structure transition. The largest relative signal change is at position 1070, where 2AP fluorescence intensity is quenched when the RNA folds, but is subsequently enhanced when L11 binds. Given the absence of a large change in the fluorescence intensity either at a single 2AP site or indeed at all sites, we posit that the binding of L11 CTD does not promote a large-scale conformational change of the RNA.

NMR

By using selective labels in the GAC, we can look directly at the environment of specific nucleobases. While the picture is still a solution average of the structure, it allows detection of conformational sampling that is not observable by SAXS or fluorescence. Since we have characterized the folding states of the GAC as ensembles of structures, we use these labeled RNAs to probe if/how the ensemble responds to L11 CTD binding.

A GAC construct was synthesized with four ^{15}N-labeled nucleotides: U1060, U1065, G1071, and U1082 (Fig. 7A and B), to report on formation of tertiary interactions [37,38]. In GAC RNA crystal structures, these nucleotides use their imino hydrogens (imino protons, $^{1}H_N$) to make tertiary hydrogen bonds: U1060 makes a Hoogsteen pair with A1088 to anchor the junction; U1065 forms a sheared base pair with A1073 to close L43, but its imino proton is proximal to A1069C2′ OH; U1082 makes a reverse Watson-Crick pair with A1086 to close the triloop; and G1071 makes a base triple with G1092:C1100 in H44 to anchor the two hairpins. Nucleobase imino protons are in exchange with solvent protons, so unless they are protected through hydrogen bonding, they are not observed in ^{1}H NMR experiments in $^{1}H_2O$. When GAC forms the predicted tertiary structure, these four specific imino protons should form tertiary hydrogen bonds and thus be observed in NMR experiments if the interactions are stable. In the spectra of the folded GAC RNA, we therefore expected to see

four peaks, each corresponding to a labeled nucleotide, as a signature of tertiary structure folding.

Looking first at the selectively labeled GAC secondary structure by ^{15}N-^{1}H SO-FAST HMQC experiments, we observed imino protons from two U's and from G1071 at 10 °C (Fig. 7C; identified by their characteristic ^{15}N chemical shifts). The appearance of a resonance (13.4 ppm) from G1071 in L43 is puzzling, since it indicates that this imino proton is protected from solvent exchange. Currently, we have no insight into any loop structure that would sequester this proton; previous hydroxyl radical cleavage of the GAC secondary structure does not provide evidence for an alternative secondary structure that would involve G1071 [18,39]. The resonances from U's are assigned to U1060 and U1065, which in the secondary structure are in H43. U1065 could form a Watson-Crick base pair with A1073 to form the L43 loop-closing U:A base pair, while U1060 could make a noncanonical U:U pair with U1078. The proton chemical shifts at 13.8 ppm and 11.2 ppm, respectively, are consistent with these pairings for U1065 and U1060. Further, these resonances indicate that in the secondary structure, the L43 stem is stacked and stable at 10 °C.

Upon addition of Mg^{2+}, we see new imino resonances appear, consistent with a conformational change of the GAC. At 10 °C in 1 mM Mg^{2+}, we see that five imino proton resonances from U's: U1060 and U1065 in the H43 duplex are still visible, while new resonances at 14.5, 12.3, and 9.5 ppm ^{1}H are present. The resonance at 9.5 ppm ^{1}H is the most intense, and its frequency indicates that this is a noncanonical base interaction. We assigned it to U1065^{37}, whose imino proton is juxtaposed to the C2′ OH of A1069 in the crystal structure (**PDB ID 6PRV**). There are also now two peaks from G1071: we assign the new one at 11.2 ppm ^{1}H to the base triple with H44. In 3 mM Mg^{2+}, the original peak at 13.4 ppm from G1071 is split, and the new peak has become very weak. At 8 mM Mg^{2+}, there are only two very weak U imino resonances at 14.1 and 9.5 ppm ^{1}H, which we think is caused by slow tumbling and intermediate exchange. Overall, these data show that some of the GAC has adopted its expected tertiary structure, but some has not, and there appears to be alternative (currently uncharacterized) structures present at 10 °C.

The GAC imino protons at 30 °C provide more insight into its structures. This temperature is below the thermal denaturation temperature of the entire RNA, but it could destabilize H43 with its many noncanonical base pairs. In fact, at 30 °C, in the absence of Mg^{2+}, only the resonance from G1071 is observed; those from U's are gone, presumably because those base pairs have been disrupted. In the presence of 1 mM Mg^{2+}, there are three U imino protons, which were also present at 10 °C in 1 mM Mg^{2+}. There are now two peaks from G1071: the one near 13.2 ppm ^{1}H is a doublet (this is not due to incomplete decoupling) indicating two environments of this proton. At 5 and 8 mM Mg^{2+}, the spectra show a strong G1071 peak at 11.1 ppm ^{1}H, yet also show a very weak peak at 13.2 ppm. The U1065 peak at 9.5 ppm ^{1}H remains strong, while a new strong U proton resonance appears at 14.1 ppm and a weak one at 12.2 ppm. In summary, GAC RNA alone in 8 mM Mg^{2+} at 30 °C has four strong imino proton peaks, as predicted, but also retains resonances from the secondary structure and at least one additional U imino proton. Thus, these data indicate that there is more than one

structure in solution in these conditions, although one is dominant. These data support our model of structural ensembles of the GAC during its folding trajectory.

Addition of *Tth* L11 CTD alters the $^{1}H/^{15}N$-HMQC spectra of the GAC RNA. Now, in the absence of Mg^{2+}, there are no peaks observed from GAC imino protons (Fig. 7C). Upon addition of 1 mM $MgCl_2$, we observed three U imino proton resonances: at 15.1 ppm (very weak) and two strong peaks at 14.7 ppm and 9.5 ppm ^{1}H. One G1071 imino resonance is present at 11.3 ppm ^{1}H. Analyses of these NMR spectra lead to two main conclusions. First, the imino proton peaks in the spectrum of GAC + L11 CTD correspond precisely to three of the four most intense peaks in the sample of GAC alone, suggesting that those two fully folded tertiary structures are essentially the same. Second, we conclude that L11 CTD binding suppresses formation of a minor population with an alternative GAC tertiary structure.

Kinetics of *Bst* L11 CTD binding

Stopped-flow fluorescence

We used rapid mixing (~1 ms dead time) with stopped-flow fluorescence to measure the association kinetics of *Bst* L11 CTD with GAC to better understand the binding mechanism. Folding of 1070AP GAC, which had the largest absolute change in fluorescence ± L11 in a background of Mg^{2+} (Fig. 5), was measured as this position and would be able to act as the most optimal probe of the RNA ensemble during the interaction. Our first experiments measured the change in fluorescence as a function of time, with different concentrations of the L11 CTD and a constant GAC concentration with 3 mM Mg^{2+} to stabilize the GAC RNA tertiary fold (Fig. 8). The data traces were fit to a sum of three exponentials to calculate the observed rates, k_{obs}, of the state transitions as binding reached equilibrium.

The relationship between observed rates and concentration of L11 can reveal further information about the mechanism of binding. The most rapid observed rate linearly increases with L11 concentration (Fig. 8), which suggests that this rate reports directly on a binding reaction. This is a classic indication of binding under pseudo-first-order conditions, where in a fit of the data to a linear function using 1 μM, 5 μM, and 10 μM data points, the slope of the line yields the observed rate of binding, $k_{on} = 2.7\ \mu M^{-1}s^{-1}$, and the intercept gives the observed dissociation rate, $k_{off} = 1.0\ s^{-1}$. The ratio gives an effective K_D of 370 nM. This calculation is in poor agreement with the affinity that we measured by nitrocellulose filter binding under similar conditions (175 mM KCl, 5 mM $MgCl_2$; $K_D = 3.8 \pm 0.7$ nM) and with ITC determination of $K_D = 40$ nM (in 100 mM KCl, 3 mM $MgCl_2$). We can understand the apparent discrepancy by consideration of the difference in what the experiments represent: The equilibrium-based experiments only report on the fraction of the L11 bound to the RNA, whereas the kinetic experiments only report on the initial binding event. So, if the rate of L11 binding differs between multiple RNA states (i.e., conformational ensembles), then the apparent K_D will differ from the measured K_D. The different results strongly support our hypothesis that the L11 protein is bound to the GAC RNA in multiple conformations.

The two slower observed rates increase as a function of L11 concentration until they plateau at ~1 μM L11. These limiting values of k_{obs} are remarkably close to the rates of the two slowest conformational transitions of Mg^{2+}-induced GAC tertiary folding in stopped-flow experiments (mixing with Mg^{2+}) [21]. The two experiments could therefore be reporting on the same conformational transitions, indicating that the GAC structure is evolving even as L11 is bound.

These data reveal an important feature of the GAC RNA:L11 complex: binding and folding equilibria are coupled. The individual *observed* rates are actually complex convolutions of multiple rate constants. This aspect of complex kinetics is rather unintuitive. An example of such coupled equilibria is explicitly elucidated in the formalism of Vogt & Di Cera [40], illustrating how observed rates of protein isomerization respond to different concentrations of bound ligand. Notably, in that treatment, they also note the correspondence between conformational selection and induced fit, although here we do not invoke either as a binding mechanism.

Our model of GAC ion-dependent folding has four intermediate states in the transition from secondary structure to tertiary fold. It is possible that L11 CTD could bind to these states and so direct the folding pathway. A second type of stopped-flow experiment (Fig. 9) was used to provide this information. First, L11 CTD was mixed with GAC in the absence of Mg^{2+}. Fitting this trace gave a very slow (~10 s) relaxation time, eliminating the scenario of L11 interaction with the GAC before Mg^{2+} associates (Mg^{2+} will initiate GAC folding in < ms [21]). Based on our previous analyses, we next mixed 3 mM Mg^{2+} together with a large excess of L11 CTD (60 μM) over the GAC RNA (100 nM). Binding of L11 CTD occurs with a rate of 168 s^{-1} (0.005 s relaxation time) in these experimental conditions, so in this regime, the GAC RNA will quickly react to the Mg^{2+} ions and will start progressing down its ion-induced folding pathway. As soon as the ensemble of GAC states reaches an L11 binding competent state, the vast excess of L11 will drive its binding. By comparing these time-resolved data to the Mg^{2+}-induced folding data, we find that the two traces deviate on the ~100 ms timescale and thus identify the L11 binding event (Fig. 9). Calculating the population of intermediates during the Mg^{2+}-induced folding trace (using the kinetic formalism described in Welty et al., 2018 [21]) reveals that the deviation in the presence of L11 is on the same timescale as the formation of the intermediate I_4. These data thus provide strong evidence that I_4 is the first (but not necessarily only) L11 binding competent state.

Building a binding model

Based on our previous studies of GAC RNA folding [21] and the collective findings presented in this work, our model of GAC folding is presented in Fig. 10. Ion association occurs first in <1 ms (2° + Mg^{2+}) and next in 50–100 ms to I_2. Now, we add L11 binding to this folding model, as shown in the binding mechanism that best describes our L11 data. States I_3, I_4, and 3° correspond to states in the Mg^{2+}-folding path. To deduce the simplest binding model, we need to factor in observations from all experiments.

1. We know from the number of observed rates calculated in kinetic binding experiments that there is a minimum of four states that are occupied during the binding reaction.

2. The difference in the apparent kinetic dissociation constant and the measured K_D from nitrocellulose filter binding and ITC suggests that there are at least two states bound to the L11 protein. The equilibrium-based experiments only report on the fraction of the L11 bound to the RNA, whereas the kinetic experiments only report on the initial binding event. So, if the rate of L11 binding differs between multiple RNA states (i.e., conformational ensembles), then the apparent K_D will differ from the measured K_D. By this reasoning, the discrepancy further supports the hypothesis that L11 binds to at least two discrete GAC RNA conformational ensembles.

3. The similarity of the two slower observed rates to those observed in Mg^{2+}-induced GAC folding suggests that the binding pathway and the folding pathway share some of the same transitions. Binding and folding are coupled in our experiments, which could also be true in cells if the concentrations of rRNA and protein are appropriate, and their encounter occurs during the RNA folding trajectory.

4. The intermediate I_3 and prior states in the pathway are not capable of binding L11 CTD on a relevant timescale.

5. The GAC tertiary folds (I_3, I_4, and 3°) are not single structures: they are ensembles that vary with Mg^{2+} concentration.

6. The dominant tertiary structure contains two bound Mg^{2+} ions and one K^+, as seen in the crystal structure of the protein-free GAC.

To test whether different models would fit our data, we employed a multiobjective genetic algorithm [21]. In brief, this framework allows us to simulate fluorescence time-courses for any given model. The simulated time-courses are compared to the experimental data for hundreds of sets of rate constants. The algorithm then uses a computational heuristic to intelligently select new sets of rate constants to test, and this process is iterated through multiple rounds. By starting with simplistic models and progressively ruling out models that underfit the data, we can select the simplest model consistent with the experiment.

The first model we tested was similar to that shown in Fig. 10, except that we removed the L11*3° state. This model contains the minimum number of potential states but was unable to fit the data. We then independently removed k_4 (the connection between 3° and L11*3°), but this model also failed. Only the complete model proved adequate, and it was tuned to improve the fit. We fixed k_1 and k_2 with values from our Mg^{2+}-induced folding pathway, constraining the heuristic to change only k_3 through k_5, while allowing only those solutions that gave rates that obeyed detailed balance. Finally, we constrained the heuristic to agree with the dissociation constant determined from *in vitro* binding data (i.e., the equilibrium populations of bound/free states). There were numerous sets of rate constants that fit the data equally well so we cannot propose a single set of rate constants for these transitions. However, the critical finding here is that this model was able to simulate traces that fit the data, indicating that there are at least two states of bound L11/GAC complexes.

Discussion

GAC in the ribosome

In cells, we imagine that the 58 nt GAC RNA first encounters K^+ and Mg^{2+} ions as it cotranscriptionally folds into its secondary structure and then uses those Mg^{2+} ions to facilitate formation of its tertiary structure. Folding of the GAC RNA is likely to occur before any encounter with L11, given the intracellular concentrations of ions. A misfolded secondary structure could prevent folding of the correct tertiary structure, and a misfolded tertiary structure could persist in the ribosome. If the GAC domain is not folded correctly, it could prevent sequence-specific contacts with EF-G, EF-Tu, or release factor, thus impeding or preventing ribosome function. As we have found, the presence of L11 favors the correct folding of the GAC during its folding trajectory. It is possible that because the GAC structures are not static, L11 could redirect an incorrectly folded RNA. *B. megaterium* lacking L11 have a slow growth phenotype and inefficient ribosome activity [41], and *S cerevisiae* lacking L11 (L12 in eukaryotes) also grow slowly [42], which could be a consequence of structural instability of the GAC domain and subsequent functional deficiency.

RNA folding and protein binding

The interplay of RNA, ions, and proteins is a fundamental property of biological systems. In general, ions neutralize the RNA backbone phosphate charges and, especially in RNA tertiary structures, divalent ions are effective at shielding regions of high negative charge density. Proteins often bind to specific sequences or structures of RNA and may depend on ions to first fold the RNA. However, examples of Group I intron folding showed that ions alone do not prevent misfolding of the RNA [43–45]. For RNAs that depend on subsequent protein binding, such a misfold could prevent formation of a productive complex. In contrast, protein binding to an unfolded RNA could act as a chaperone to direct formation of the correct structure. In this scenario, divalent ions would associate secondarily to trap the folded RNA structure in the complex. Sorting out the particular strategy of formation of an RNA/protein complex is challenging but necessary in order to understand the mechanism (especially if the goal is to disrupt or modulate it).

The intricate tertiary structure of the GAC was first seen in cocrystal structures of L11 CTD or full-length L11 bound to the 58-nucleotide GAC. Its structure contained a specifically bound K^+ ion and two Mg^{2+} ions and thus posed as an example of how RNA can use ions and protein to adopt a stable tertiary fold. Now, we show that L11 protein is not required for GAC RNA to bind ions, as it can adopt its ion-dependent tertiary structure without protein assistance. However, we also show that the protein is able to favor the correct tertiary fold along the folding pathway.

Our first experiments assessed L11 CTD association with GAC secondary structures. While it is conceivable that the ensemble of GAC secondary structures could include tertiary conformations, we did not observe any substantial specific binding, whether it be by filter binding, ITC, SAXS, NMR, or fluorescence. We conclude that the L11 CTD does not, on its

own, induce a correct fold of GAC RNA in the absence of Mg^{2+}. In this context, it is not acting as a chaperone to fold the GAC RNA.

We developed a kinetic scheme of divalent ion-induced GAC folding, based on stopped-flow fluorescence experiments. It included six states along the folding trajectory, three of which (I_3, I_4, and 3°) are populated after divalent ions have associated. NMR data describing the conformations of the GAC RNA support our model of multiple folded states: we observe that in the presence of Mg^{2+}, GAC adopts alternate conformations (which could be exchanging among each other). These conformations could be off-pathway structures that are kinetically or thermodynamically stuck. Alternatively, they could correspond to I_3 and/or I_4, which are on the pathway to the final folded structure. However, one conformation dominates the population, based on NMR experiments that probe formation of tertiary interactions.

We find that the protein binds to I_4 in the kinetic pathway and propose that it then directs GAC RNA along its correct final folding trajectory. Such direction could be steric or electrostatic or through conformational selection of the productive tertiary fold. In the presence of L11 CTD, the GAC RNA adopts a single folded conformation, based on NMR data. Crucially, NMR data indicate that the GAC tertiary structure in the presence of L11 is the dominant conformation in the absence of L11. We conclude that this structure corresponds to the crystal structure of the GAC RNA alone.

In summary, we conclude that L11 binding restricts the distribution of conformations in the ensemble of GAC folded states to the one seen in crystal structures. This finding suggests that binding of L11 ensures complete and stable folding of the GAC RNA into the necessary conformation competent to bind EF-G, RF2, and EF-Tu. L11 was shown to be critical for optimal ribosome activity, and now the molecular necessity for its association with GAC RNA is known.

Methods

Nitrocellulose filter binding

GAC RNAs were radiolabeled with 3000 Ci/mM α–^{32}P-UTP and -CTP using T7 RNA polymerase *in vitro* transcription [46] and purified by denaturing gel electrophoresis. Bands were excised, soaked overnight in 0.3 M sodium acetate, and recovered from the solution by ethanol precipitation and subsequent resuspension in MilliQ water. Aliquots were diluted ~1000 into KCl to give ~30 cpm/μL, and the GAC RNA was folded by heating at 65 °C for 30 min, then quenched on ice. L11 CTDs were incubated from 10^{-12} to 10^{-6} M concentrations with ~1 pmole RNA in reactions containing 10 μg/mL yeast tRNA, 20 μg/mL acetylated BSA (Boehringer), 10 mM sodium cacodylate pH 6.5, with different concentrations of $MgCl_2$ (3–5 mM) and KCl (100–350 mM). Samples were incubated at 22 °C for 30 min, then filtered through S&S 0.45 μm nitrocellulose filters that had been soaked with the same salts for more than an hour. RNA was quantified using a STORM phosphorimager and data processed with Kaleidagraph (Synergy software). The data were fit to a quadratic equation as described [47].

ITC experiments were performed on a TA instruments Nano-ITC calorimeter. RNA was folded by heating to 65 °C for 30 min, then on ice for an hour. L11 protein and GAC RNA were dialyzed in the same buffer before titration [100 mM KCl, 10 mM cacodylate pH 6.5]. $MgCl_2$ solutions were buffer matched to the GAC RNA solutions by dialysis. All solutions were degassed immediately prior to titration. Controls of RNA titrated into buffer and L11 titrated into buffer were carried out for all solution conditions and subtracted from the raw experimental titration data. 2.5 μl volumes of RNA were titrated into solutions containing L11 for protein binding experiments. Thermograms were processed using the NITPIC software package [48].

Fluorescence

Steady-state fluorescence experiments were performed with a Photon Technologies International spectrofluorometer. RNAs were chemically synthesized to contain a single 2AP substitution [36,38]. (*Bst* L11 CTD was used for fluorescence experiments since *Tth* L11 CTD has a tryptophan that interferes with 2-aminopurine fluorescence measurements). Protein was dialyzed into binding buffer without Mg^{2+}, while RNA was added to binding buffer from a concentrated stock solution, heated to 65 °C, and quenched on ice prior to the experiments. Samples were excited at 308 nm, fluorescence was measured at 368 nm. Data acquisition had a 1 s integration time and was averaged over 5 s. Measurements were made with 1 μm GAC RNA concentration, both ± 5 mM $MgCl_2$ and 5 mM $MgCl_2$ with 2 μM L11 protein.

Stopped-flow fluorescence measurements were made at 20 °C with an applied Photophysics SX 20 stopped-flow spectrofluorometer. The standard buffer condition was 100 mM KCl, 3 mM $MgCl_2$, 10 mM sodium cacodylate, Ph 6.5. Reported curves are the average of five or more individual time-course measurements consisting of 500 points taken uniformly over the first 5 s, and 10,000 points uniformly taken over the next 100 s. Initial concentrations: 200 nM GAC A1070AP mixed with 6 mM $MgCl_2$ or 32 μM L11 or (6 mM $MgCl_2$ and 60 μM L11 CTD). GAC RNA concentration, after mixing, was 100 nm and was in a background of standard buffer. Averaged data curves were fit with a 3-exponential equation $y = y_o + A_1 e^{\frac{-t}{\tau_1}} + A_2 e^{\frac{-t}{\tau_2}} + A_3 e^{\frac{-t}{\tau_3}}$ using the OriginPro software package. Data were also fit with our in-house genetic algorithm [21] to calculate the individual rate constants.

X-ray crystal structure determination

58nt GAC RNA was *in vitro* transcribed from linearized plasmid DNA using T7 RNA polymerase as previously described [49]. Following purification by gel filtration chromatography in 50 mM tris buffer (pH 8.5), 75 mM KCl, 5 mM $MgCl_2$, RNA (0.6 mM) was annealed at 65 °C for 10 min and allowed to cool slowly to room temperature prior to crystallization. Crystals of the free GAC RNA were obtained by vapor diffusion after mixing the RNA 1:1 with crystallization solution containing 15–20% polyethylene glycol 4000, 0.6–1.2 M NaCl, and 50 mM sodium cacodylate (pH 6.5). X-ray diffraction data were collected on beamline ID23–1 of the European Synchrotron Radiation Facility (ESRF), Grenoble, France, and were integrated and merged using XDS/XSCALE [50]. The free GAC RNA structure was determined by molecular replacement in Phenix [51] using the RNA

from the GAC RNA-L11 CTD complex structure (**PDB ID 1HC8**) as the model after removing protein and all-bound waters and ions. Waters and ions were rebuilt into the resulting maps in Coot [52] and the structure refined using Phenix [51]. Full X-ray diffraction data collection and structure refinement statistics are provided in Table 1. GAC RNA coordinates and associated maps have been deposited in the RCSB PDB under accession code **6PRV**.

NMR

^{15}N-^{1}H SO-FAST HMQC spectra [53,54] were recorded at 600 and 500 and 700 MHz (^{1}H) on Bruker Avance III and Varian Inova spectrometers, respectively. Spectral widths: 12000 Hz (^{1}H), 1600 Hz (^{15}N). Proton chemical shifts are referenced to 2,2-dimethyl-2-silapentane-5-sulfonate (DSS). ^{15}N resonances were indirectly referenced to DSS via the ^{1}H/^{15}N gyromagnetic ratio. Solutions contained 100 mM KCl, 10 mM sodium cacodylate pH 6.5, with/without $MgCl_2$ and with/without *Tth* L11 CTD, typically at 30 °C.

GAC RNA was folded to its secondary structure (heated to 65 °C for 30 min, then on ice for an hour), then its spectra recorded in 100 mM KCl, 10 mM sodium cacodylate pH 6.5, from 10° to 30 °C. ^{15}N-RNA was added into lyophilized aliquots of $MgCl_2$ (Aldrich 99.995%) to give final concentrations of 200 μM, 500 μM, 1 mM, 3 mM, and 8 mM in a 3 mm tube. After each addition, the sample was allowed to equilibrate for an hour at 20 °C, then spectra were collected at 10°, 20° and 30 °C for 12 h, in 90% H_2O, 10% D_2O. For experiments with L11 CTD, protein was added to RNA in 100 mM KCl, 10 mM sodium cacodylate, pH 6.5, then $MgCl_2$ was titrated into the sample. [GAC] = 500 μM, and [GAC] = 300 μM, [L11] = 600 μM, 90% H_2O, 10% D_2O

SAXS

The RNA molecules used in the SAXS experiments were synthesized via T7 transcription using the T7 RiboMAX Express Large-Scale RNA Production System (PROMEGA) and purified using an Anion-Exchange Column (HiTRAP DEAE FF, GE Healthcare). The *B. stearothemophilus* CTD L11 protein was overexpressed and purified from *E. coli* as described from Xing and Draper [9]. Buffer conditions for SAXS experiments were 10 mM MOPSO, 100 mM KCl, pH 6.5. Samples for SAXS were initially tested in different annealing conditions (65 °C, 70 °C, snap cool, slow cool, use as is from frozen) and different buffer conditions (MOPS, pH 7 vs. MOPSO, pH 6.5) to determine the effect on RNA folding. There was no significant difference in the data obtained, so the standard condition used was to anneal at 65 °C for 30 min and slow cool. CTD-L11 protein and/or magnesium ions in the same buffers were incubated with the RNA prior to the SAXS measurements.

All SAXS data were collected at the Cornell High Energy Synchrotron Source (CHESS) using the BioSAXS setup at the G1 beamline with X-ray energy of 9.91 keV and a beam size of 250 μm^2. To ensure homogeneity in the samples, the SAXS samples were either purified though a Size-Exclusion Column (Superdex 200 Increase 10/300 GL, GE Healthcare) prior to the static SAXS experiments (regular static SAXS setup) or pushed through the in-line Size-Exclusion Chromatography SAXS (SEC-SAXS) setup [55]. For regular static SAXS, 30 μL samples (20 μM RNA and/or 30 μM protein) were loaded in a

1.5 mm quartz capillary and the samples were oscillated to avoid radiation damage. Scattering of buffer solutions, loaded and oscillated in the same fashion as the samples, was measured in between sample sets to use for buffer subtraction. Measurements were made using the Pilatus 100K detector over 20 s with a 1 s integration time. For inline SEC-SAXS, 100 μL samples (50 μM RNA and/or 70 mM protein) were injected into a sample loop of an SEC column preincubated with buffer (Superdex 200 Increase 5/150 GL, GE Healthcare) and allowed to flow through the column at 0.27 mL/min. SAXS measurements were collected right after injection for 1200 s with a 1 s integration time using the same Pilatus 100K detector. Strong scattering signal from the molecules appears for about 60 s in the middle of the collection period and the scatterings from before and after the sample were used for buffer subtraction.

All SAXS data were processed using BioXTAS RAW [56] and in-house MATLAB scripts. The reported radii of gyrations (Rg) were calculated from a Guinier Analysis. The Kratky profiles, plots of $I \times q^2$ vs. q, are shown to emphasize shape changes in the middle- to high-q region. We find that the shape of the scattering signal is the same whether the regular static SAXS setup or inline SEC-SAXS was used, although signal-to-noise ratio was poorer for inline SEC-SAXS because of sample dilution.

GAC RNA X-ray crystal structures are deposited in the RCSB PDB under accession code **PDB ID 6PRV**.

Acknowledgements

We thank Professor Roberto Galletto (WUSM) for the use of his stopped-flow spectrometer. 2AP-GAC RNAs were received from Agilent labs, and we thank Dr. Laura-Kay Bruhn and especially Dr. Doug Dellinger for ^{15}N GAC RNAs. KBH and RW thank Professor David Draper for his gift of L11 CTD proteins. We thank members of the Pollack Lab of Cornell University and Richard Gillilan of Cornell High Energy Synchrotron Source (CHESS) for experimental assistance during SAXS measurements. Funding to LP is from the National Institutes of Health (R35-GM122514) and the National Science Foundation through a Science and Technology Center grant 1231306. CHESS is supported by the National Science Foundation award DMR-1332208, and the Macromolecular Diffraction at CHESS (MacCHESS) resource is supported by award GM-103485 from the National Institutes of Health. X-ray diffraction data collection was performed on beamline ID23-1 at the European Synchrotron Radiation Facility (ESRF), Grenoble, France, and we gratefully acknowledge the beamline staff for their assistance. This work was supported by the Wellcome Trust Grant 79242 to GLC.

References

[1]. Moazed D, Robertson JM, Noller HF, Interaction of elongation factors EF-G and EF-Tu with a conserved loop in 23S RNA, Nature 334 (1988) 362–364. [PubMed: 2455872]

[2]. Li W, Sengupta J, Rath BK, Frank J, Functional conformations of the L11-ribosomal RNA complex revealed by correlative analysis of cryo-EM and molecular dynamics simulations, RNA 12 (2006) 1240–1253. [PubMed: 16682558]

[3]. Gao Y-G, Selmer M, Dunham CM, Weixlbaumer A, Kelley AC, Ramakrishnan V, The structure of the ribosome with elongation factor G trapped in the posttranslocational state, Science 326 (2009) 694–699. [PubMed: 19833919]

[4]. Sköld SE, Chemical crosslinking of elongation factor G to the 23S RNA in 70S ribosomes from Escherichia coli, Nucleic Acids Res. 11 (1983) 4923–4932. [PubMed: 6348702]

[5]. Weixlbaumer A, Jin H, Neubauer C, Voorhees RM, Petry S, Kelley AC, Ramakrishnan V, Insights into translational termination from the structure of RF2 bound to the ribosome, Science 322 (2008) 953–956 (80-.). [PubMed: 18988853]

[6]. Egebjerg J, Douthwaite SR, Liljas A, Garrett RA, Characterization of the binding sites of protein L11 and the L10.(L12)4 pentameric complex in the GTPase domain of 23 S ribosomal RNA from Escherichia coli, J. Mol. Biol 213 (1990) 275–288. [PubMed: 1692883]

[7]. Hinck AP, Markus MA, Huang S, Grzesiek S, Kustonovich I, Draper DE, Torchia DA, The RNA binding domain of ribosomal protein L11: three-dimensional structure of the RNA-bound form of the protein and its interaction with 23 S rRNA, J. Mol. Biol 274 (1997) 101–113. [PubMed: 9398519]

[8]. Xing Y, Guha Thakurta D, Draper DE, The RNA binding domain of ribosomal protein L11 is structurally similar to homeodomains, Nat. Struct. Biol 4 (1997) 24–27. [PubMed: 8989317]

[9]. Xing Y, Draper DE, Cooperative interactions of RNA and thiostrepton antibiotic with two domains of ribosomal protein L11, Biochemistry 35 (1996) 1581–1588. [PubMed: 8634289]

[10]. Jonker HRA, Ilin S, Grimm SK, Wöhnert J, Schwalbe H, L11 domain rearrangement upon binding to RNA and thiostrepton studied by NMR spectroscopy, Nucleic Acids Res. 35 (2007) 441–454. [PubMed: 17169991]

[11]. Xing Y, Draper DE, Stabilization of a ribosomal RNA tertiary structure by ribosomal protein L11, J. Mol. Biol 249 (1995) 319–331. [PubMed: 7783196]

[12]. el-Baradi TT, de Regt VC, Einerhand SW, Teixido J, Planta RJ, Ballesta JP, Raué HA, Ribosomal proteins EL11 from Escherichia coli and L15 from Saccharomyces cerevisiae bind to the same site in both yeast 26 S and mouse 28 S rRNA, J. Mol. Biol 195 (1987) 909–917. [PubMed: 3309345]

[13]. Thompson J, Musters W, Cundliffe E, Dahlberg AE, Replacement of the L11 binding region within E.coli 23S ribosomal RNA with its homologue from yeast: in vivo and in vitro analysis of hybrid ribosomes altered in the GTPase centre, EMBO J. 12 (1993) 1499–1504. [PubMed: 7682175]

[14]. Maklan EJ, Genetic and biochemical analysis of the GTPase associated center of the ribosome. UC Santa Cruz, 2012, http://escholarship.org/uc/item/7gh9v43, 2012.

[15]. Xu W, Pagel FT, Murgola EJ, Mutations in the GTPase center of Escherichia coli 23S rRNA indicate release factor 2-interactive sites, J. Bacteriol 184 (2002) 1200–1203. [PubMed: 11807083]

[16]. Arkov AL, Freistroffer DV, Ehrenberg M, Murgola EJ, Mutations in RNAs of both ribosomal subunits cause defects in translation termination, EMBO J. 17 (1998) 1507–1514. [PubMed: 9482747]

[17]. Laing LG, Gluick TC, Draper DE, Stabilization of RNA structure by Mg ions. Specific and non-specific effects, J. Mol. Biol 237 (1994) 577–587. [PubMed: 8158638]

[18]. Leipply D, Draper DE, Evidence for a thermodynamically distinct Mg2+ ion associated with formation of an RNA tertiary structure, J. Am. Chem. Soc 133 (2011) 13397–13405. [PubMed: 21776997]

[19]. Ryan PC, Draper DE, Detection of a key tertiary interaction in the highly conserved GTPase center of large subunit ribosomal RNA, Proc. Natl. Acad. Sci. U.S.A 88 (1991) 6308–6312. [PubMed: 2068110]

[20]. Bukhman YV, Draper DE, Affinities and selectivities of divalent cation binding sites within an RNA tertiary structure, J. Mol. Biol 273 (1997) 1020–1031. [PubMed: 9367788]

[21]. Welty R, Pabit SA, Katz AM, Calvey GD, Pollack L, Hall KB, Divalent ions tune the kinetics of a bacterial GTPase center rRNA folding transition from secondary to tertiary structure, RNA 24 (2018) 1828–1838. [PubMed: 30254137]

[22]. Lee D, Walsh JD, Yu P, Markus MA, Choli-Papado-poulou T, Schwieters CD, Krueger S, Draper DE, Wang Y-X, The structure of free L11 and functional dynamics of L11 in free, L11-rRNA(58 nt) binary and L11-rRNA(58 nt)-thiostrepton ternary complexes, J. Mol. Biol 367 (2007) 1007–1022. [PubMed: 17292917]

[23]. Wimberly BT, Guymon R, McCutcheon JP, White SW, Ramakrishnan V, A detailed view of a ribosomal active site: the structure of the L11-RNA complex, Cell 97 (1999) 491–502. [PubMed: 10338213]

[24]. Conn GL, Gittis AG, Lattman EE, Misra VK, Draper DE, A compact RNA tertiary structure contains a buried backbone-K+ complex, J. Mol. Biol 318 (2002) 963–973. [PubMed: 12054794]

[25]. Lu M, Draper DE, On the role of rRNA tertiary structure in recognition of ribosomal protein L11 and thiostrepton, Nucleic Acids Res. 23 (1995) 3426–3433. [PubMed: 7567452]

[26]. Ryan PC, Draper DE, Thermodynamics of protein-RNA recognition in a highly conserved region of the large-subunit ribosomal RNA, Biochemistry 28 (1989) 9949–9956. [PubMed: 2620068]

[27]. Blyn LB, Risen LM, Griffey RH, Draper DE, The RNA-binding domain of ribosomal protein L11 recognizes an rRNA tertiary structure stabilized by both thiostrepton and magnesium ion, Nucleic Acids Res. 28 (2000) 1778–1784. [PubMed: 10734197]

[28]. GuhaThakurta D, Draper DE, Contributions of basic residues to ribosomal protein L11 recognition of RNA, J. Mol. Biol 295 (2000) 569–580. [PubMed: 10623547]

[29]. Markus MA, Hinck AP, Huang S, Draper DE, Torchia DA, High resolution solution structure of ribosomal protein L11-C76, a helical protein with a flexible loop that becomes structured upon binding to RNA, Nat. Struct. Biol 4 (1997) 70–77. [PubMed: 8989327]

[30]. GuhaThakurta D, Draper DE, Protein-RNA sequence covariation in a ribosomal protein-rRNA complex, Biochemistry 38 (1999) 3633–3640. [PubMed: 10090750]

[31]. Harms JM, Wilson DN, Schluenzen F, Connell SR, Stachelhaus T, Zaborowska Z, Spahn CMT, Fucini P, Translational regulation via L11: molecular switches on the ribosome turned on and off by thiostrepton and micrococcin, Mol. Cell 30 (2008) 26–38. [PubMed: 18406324]

[32]. Valle M, Zavialov A, Li W, Stagg SM, Sengupta J, Nielsen RC, Nissen P, Harvey SC, Ehrenberg M, Frank J, Incorporation of aminoacyl-tRNA into the ribosome as seen by cryo-electron microscopy, Nat. Struct. Biol 10 (2003) 899–906. [PubMed: 14566331]

[33]. Lu M, Draper DE, Bases defining an ammonium and magnesium ion-dependent tertiary structure within the large subunit ribosomal RNA, J. Mol. Biol 244 (1994) 572–585. [PubMed: 7527467]

[34]. Ryan PC, Lu M, Draper DE, Recognition of the highly conserved GTPase center of 23 S ribosomal RNA by ribosomal protein L11 and the antibiotic thiostrepton, J. Mol. Biol 221 (1991) 1257–1268. [PubMed: 1942050]

[35]. Pollack L, SAXS studies of ion-nucleic acid interactions, Annu. Rev. Biophys 40 (2011) 225–242. [PubMed: 21332357]

[36]. Welty R, Hall KB, Nucleobases undergo dynamic rearrangements during RNA tertiary folding, J. Mol. Biol 428 (2016) 4490–4502. [PubMed: 27693721]

[37]. Rau MJ, Welty R, Tom Stump W, Hall KB, formation of tertiary interactions during rRNA GTPase center folding, J. Mol. Biol 427 (2015) 2799–2815. [PubMed: 26210661]

[38]. Dellinger DJ, Timár Z, Myerson J, Sierzchala AB, Turner J, Ferreira F, Kupihár Z, Dellinger G, Hill KW, Powell JA, Sampson JR, Caruthers MH, Streamlined process for the chemical synthesis of RNA using 2'-O-thionocarbamate-protected nucleoside phosphoramidites in the solid phase, J. Am. Chem. Soc 133 (2011) 11540–11556. [PubMed: 21688829]

[39]. Lambert D, Leipply D, Draper DE, The osmolyte TMAO stabilizes native RNA tertiary structures in the absence of Mg2+: evidence for a large barrier to folding from phosphate dehydration, J. Mol. Biol 404 (2010) 138–157. [PubMed: 20875423]

[40]. Vogt AD, Di Cera E, Conformational selection is a dominant mechanism of ligand binding, Biochemistry 52 (2013) 5723–5729. [PubMed: 23947609]

[41]. Stark M,Cundliffe E, Onthe biologicalroleofribosomalprotein BM-L11 of Bacillus megaterium, homologous with Escherichia coli ribosomal protein L11, J. Mol. Biol 134 (1979) 767–769. [PubMed: 119869]

[42]. Briones E, Briones C, Remacha M, Ballesta JPG, The GTPase center protein L12 is required for correct ribosomal stalk assembly but not for Saccharomyces cerevisiaeViability, J. Biol. Chem 273 (1998) 31956–31961. [PubMed: 9822666]

[43]. Russell R, Das R, Suh H, Travers KJ, Laederach A, Engelhardt MA, Herschlag D, The paradoxical behavior of a highly structured misfolded intermediate in RNA folding, J. Mol. Biol 363 (2006) 531–544. [PubMed: 16963081]

[44]. Xue Y, Gracia B, Herschlag D, Russell R, Al-Hashimi HM, Visualizing the formation of an RNA folding intermediate through a fast highly modular secondary structure switch, Nat. Commun 7 (2016) ncomms11768.

[45]. Rangan P, Masquida B, Westhof E, Woodson SA, Architecture and folding mechanism of the Azoarcus Group I pre-tRNA, J. Mol. Biol 339 (2004) 41–51. [PubMed: 15123419]

[46]. Milligan JF, Groebe DR, Witherell GW, Uhlenbeck OC, Oligoribonucleotide synthesis using T7 RNA polymerase and synthetic DNA templates, Nucleic Acids Res. 15 (1987) 8783–8798. [PubMed: 3684574]

[47]. Hall KB, Kranz JK, Thermodynamics and mutations in RNA-protein interactions, Methods Enzymol. 259 (1995) 261–281. [PubMed: 8538458]

[48]. Keller S, Vargas C, Zhao H, Piszczek G, Brautigam CA, Schuck P, High-precision isothermal titration calorimetry with automated peak-shape analysis, Anal. Chem 84 (2012) 5066–5073. [PubMed: 22530732]

[49]. Dunstan MS, Guhathakurta D, Draper DE, Conn GL, Coevolution of protein and RNA structures within a highly conserved ribosomal domain, Chem. Biol 12 (2005) 201–206. [PubMed: 15734647]

[50]. Kabsch W, Automatic processing of rotation diffraction data from crystals of unknown symmetry and cell constants, J. Appl. Crystallogr 26 (1993) 795–800.

[51]. Adams PD, Afonine PV, Bunkóczi G, Chen VB, Davis IW, Echols N, Headd JJ, Hung L-W, Kapral GJ, Grosse-Kunstleve RW, McCoy AJ, Moriarty NW, Oeffner R, Read RJ, Richardson DC, Richardson JS, Terwilliger TC, Zwart PH, PHENIX : a comprehensive Python-based system for macromolecular structure solution, Acta Crystallogr. Sect. D Biol. Crystallogr 66 (2010) 213–221. [PubMed: 20124702]

[52]. Emsley P, Cowtan K, Coot: model-building tools for molecular graphics, Acta Crystallogr. Sect. D Biol. Crystallogr 60 (2004) 2126–2132. [PubMed: 15572765]

[53]. Schanda P, Brutscher B, Very fast two-dimensional NMR spectroscopy for real-time investigation of dynamic events in proteins on the time scale of seconds, J. Am. Chem. Soc 127 (2005) 8014–8015. [PubMed: 15926816]

[54]. Schanda P, Forge V, Brutscher B, HET-SOFAST NMR for fast detection of structural compactness and heterogeneity along polypeptide chains, Magn. Reson. Chem 44 (2006) S177–S184. [PubMed: 16823898]

[55]. Trewhella J, Duff AP, Durand D, Gabel F, Guss JM, Hendrickson WA, Hura GL, Jacques DA, Kirby NM, Kwan AH, Pérez J, Pollack L, Ryan TM, Sali A, Schneidman-Duhovny D, Schwede T, Svergun DI, Sugiyama M, Tainer JA, Vachette P, Westbrook J, Whitten AE, 2017 publication guidelines for structural modelling of small-angle scattering data from biomolecules in solution: an update, Acta Crystallogr. Sect. D. Struct. Biol 73 (2017) 710–728. [PubMed: 28876235]

[56]. Hopkins JB, Gillilan RE, Skou S, BioXTAS RAW: improvements to a free open-source program for small-angle X-ray scattering data reduction and analysis, J. Appl. Crystallogr 50 (2017) 1545–1553. [PubMed: 29021737]

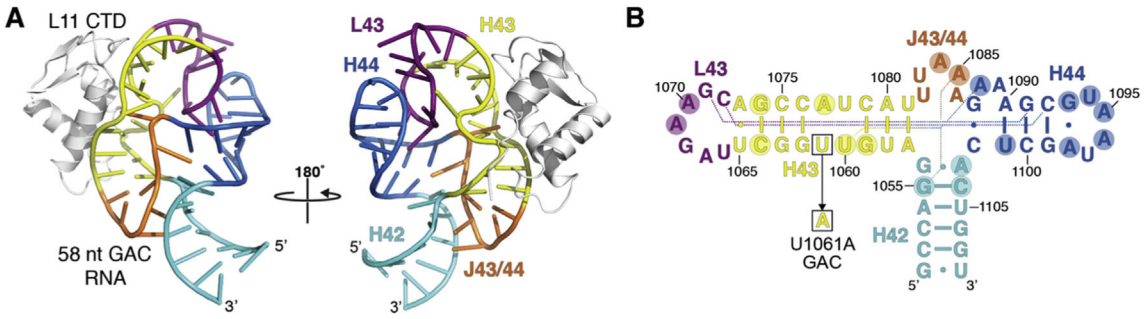

Fig. 1. Crystal structure of the GAC RNA:L11-CTD complex.

A, Cartoon of the *E. coli* GAC RNA with U1061A mutation bound to *B. stearothermophilus* L11-CTD (**PDB ID 1HC8**) [24]. ***B***. Secondary structure of the *E. coli* GAC U1061A RNA with helices and loop sequence color-coded to match the structural elements in the tertiary structure. Invariant nucleotides (circled) and select long-range hydrogen bonds (dotted lines) are also indicated. The mutated residue generating the U1061A GAC variant is also indicated.

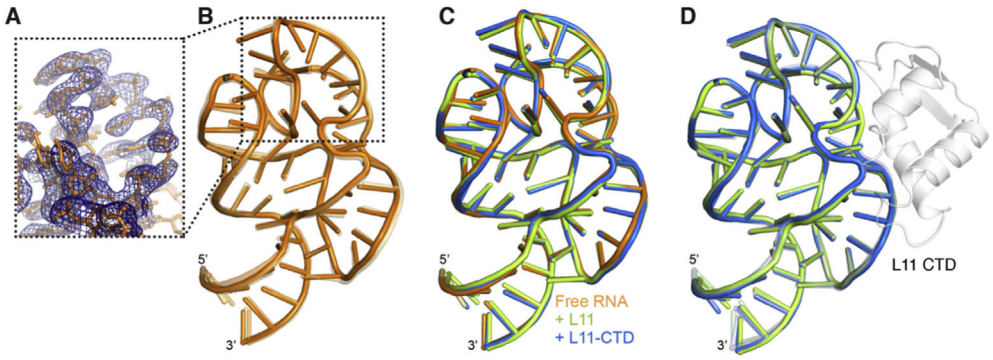

Fig. 2. Structure of the free GAC RNA.

A. Example 2mFo-DFc composite omits electron density map for a region of the free GAC RNA model (nts 1065–1073). Structural superpositions of **B.** The three copies of free GAC (chains A-C, **PDB ID 6PRV**; orange); **C.** free, L11-CTD-bound (**PDB ID 1HC8**; blue), and full-length L11-bound (**PDB ID 1MMS**; green) GAC RNA; and **D**. L11-CTD and L11 bound GAC RNA structures. In all alignments, one molecule in the corresponding PDB for each structure is shown as solid cartoon and other chains as semitransparent cartoons.

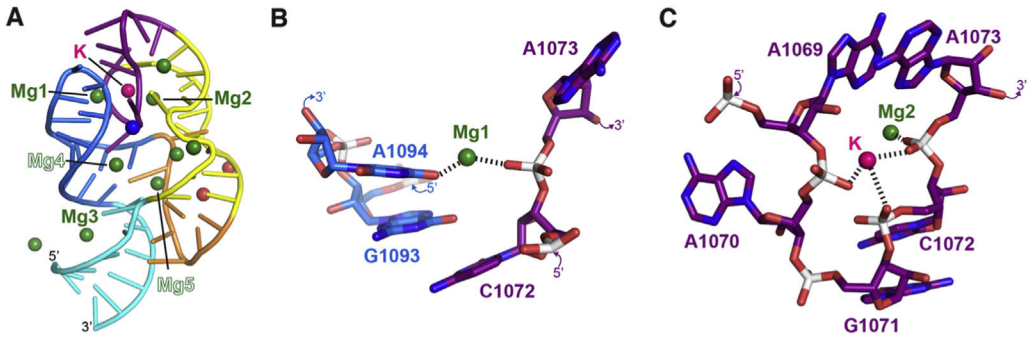

Fig. 3. Modeled ions in the free GAC structure.

A. Locations of Mg^{2+} and K^{+} ions in chain A and additional unique locations in chains B and C of the free GAC structure are shown as color-coded spheres. All Mg^{2+} bound to chain A are shown and colored green; for chains B and C, only additional unique positions are shown, colored blue and red, respectively. The labeled ions are bound in all three copies of the free GAC RNA (K, Mg1, Mg2 and Mg3) or bound in chain A and either chain B or chain C (Mg4 and Mg5, respectively). **B**. Detailed view of Mg1 bridging GAC RNA regions (L43 and H44) distant in the primary sequence but brought into close proximity by the RNA tertiary structure. **C**. Detailed view of Mg^{2+} (Mg2) and K^{+} coordination within the unusual tertiary conformation of GAC L43.

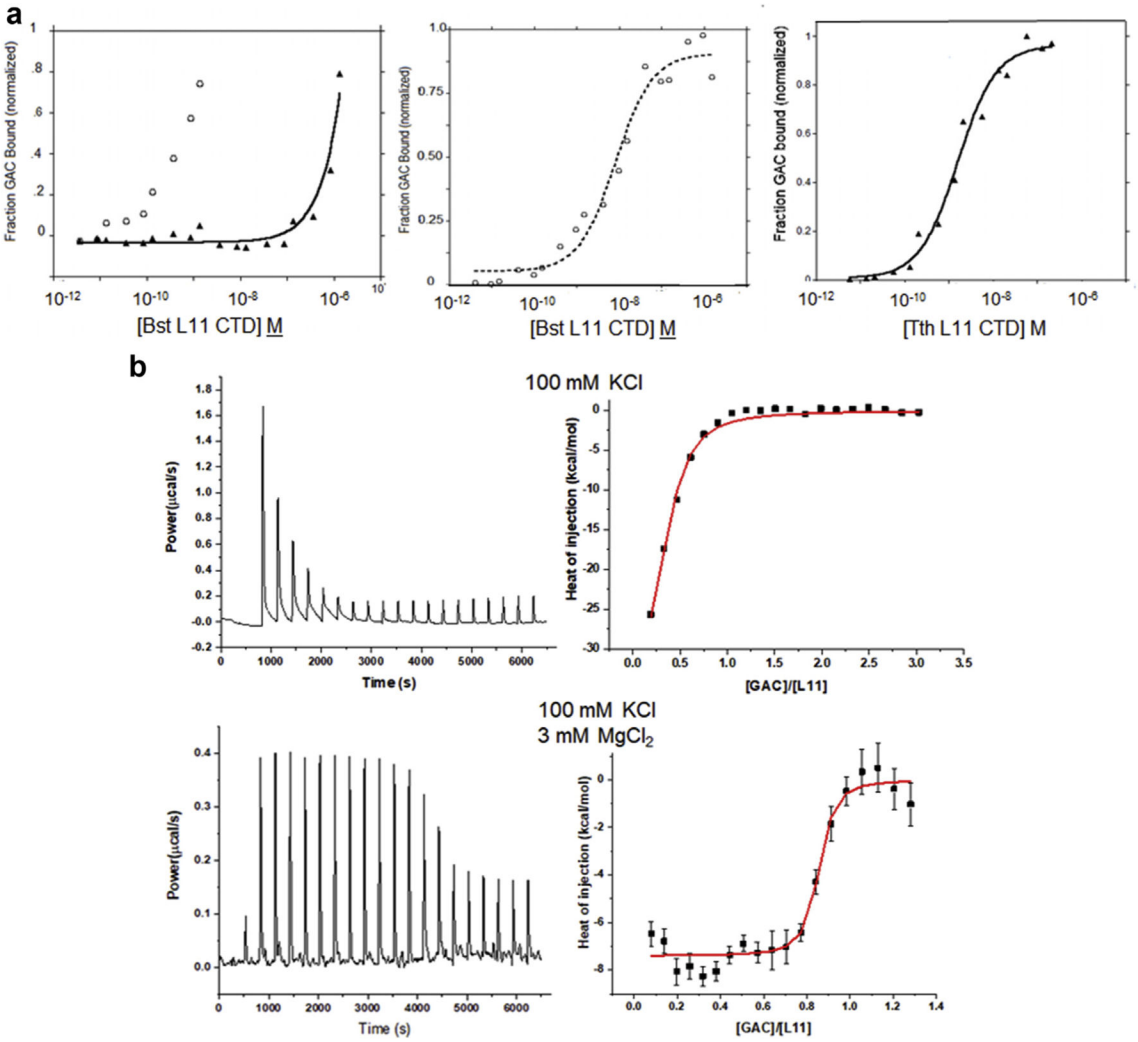

Fig. 4. Binding modes in the absence and presence of divalent ion.

A. Nitrocellulose filter binding experiments with GAC U1061A. left: *Bst* L11 CTD in 100 mM KCl (■) and with addition of 8 mM Mg^{2+} (▫). Mid: *Bst* L11 CTD in 300 mM KCl, 8 mM $MgCl_2$, 10 mM sodium cacodylate, pH 6.5, K_D = 8 ± 2 nM; right: *Tth* L11 CTD in 300 mM KCl, 8 mM $MgCl_2$, 10 mM sodium cacodylate, pH 6.5, K_D = 1.6 ± 0.3 nM. **B**. ITC isotherms and thermograms for titrations of the GAC RNA into *Tth* L11 CTD in 100 mM KCl ±3 mM $MgCl_2$. For KCl titrations, L11 CTD was 22 µM and for $MgCl_2$ titrations, it was 20 µM. The RNA concentration in the injection syringe was 200 µm and 77 mm for KCl and $MgCl_2$ experiments, respectively.

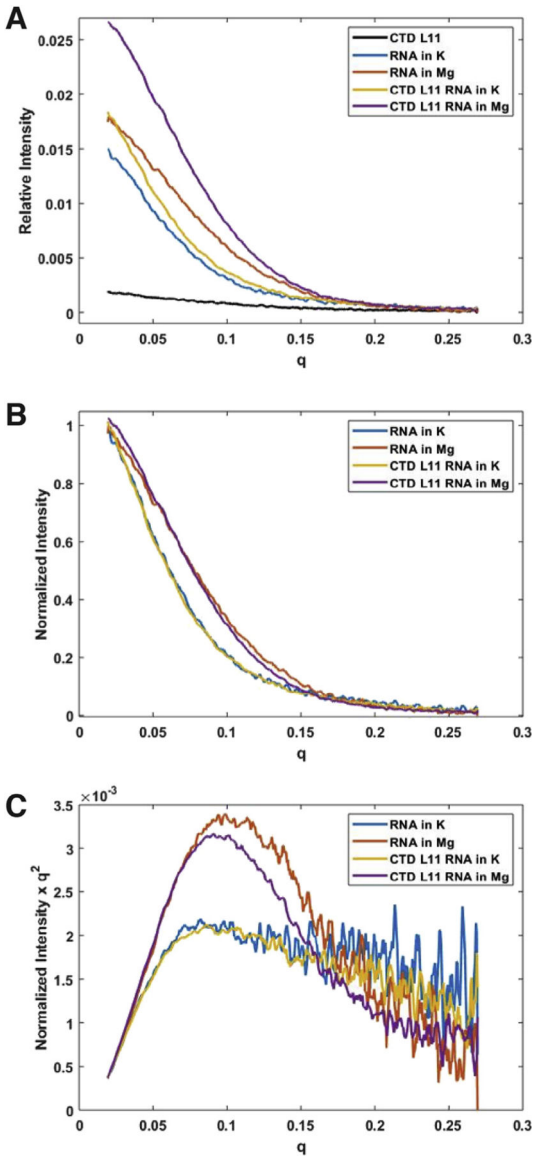

Fig. 5. Small-angle X-ray scattering profiles of GAC RNA.

A. Relative scattering intensities of the protein, RNA alone and RNA with protein. **B**. Normalized scattering intensity of unfolded GAC RNA in KCl (blue) is unchanged by addition of *Bst* L11 CTD (yellow-orange). Likewise, scattering intensity of tertiary-folded GAC RNA in 1 mM $MgCl_2$ is relatively unchanged by addition of protein. **C**. Kratky plots of the data show the characteristic plateau of an extended structure for GAC RNA in KCl, with or without L11, while the bell-shaped curve indicates a more globular RNA fold in Mg^{2+} with or without L11. To ensure that we were measuring scattering from the intact L11/GAC complex, we prepared the complex by size-exclusion chromatography before SAXS acquisition.

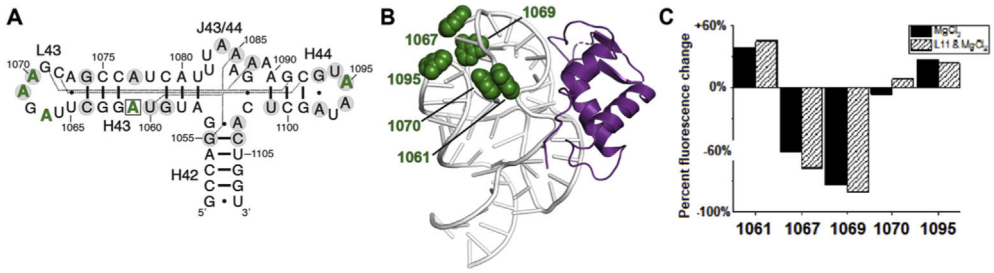

Fig. 6. GAC-2AP fluorescence ± L11 CTD.

A. Locations of the 2AP sites in the GAC secondary structure (green letters) and ***B***. Mapped (green spheres) onto the cocrystal of *E. coli* U1061A GAC RNA (white) bound by *Tth* L11 CTD (purple) (**PDB ID 1HC8**). ***C***. 2AP fluorescence intensity change of folded GAC when *Bst* L11 CTD is bound, compared to initial fluorescence change due to Mg^{2+}-dependent tertiary structure formation.

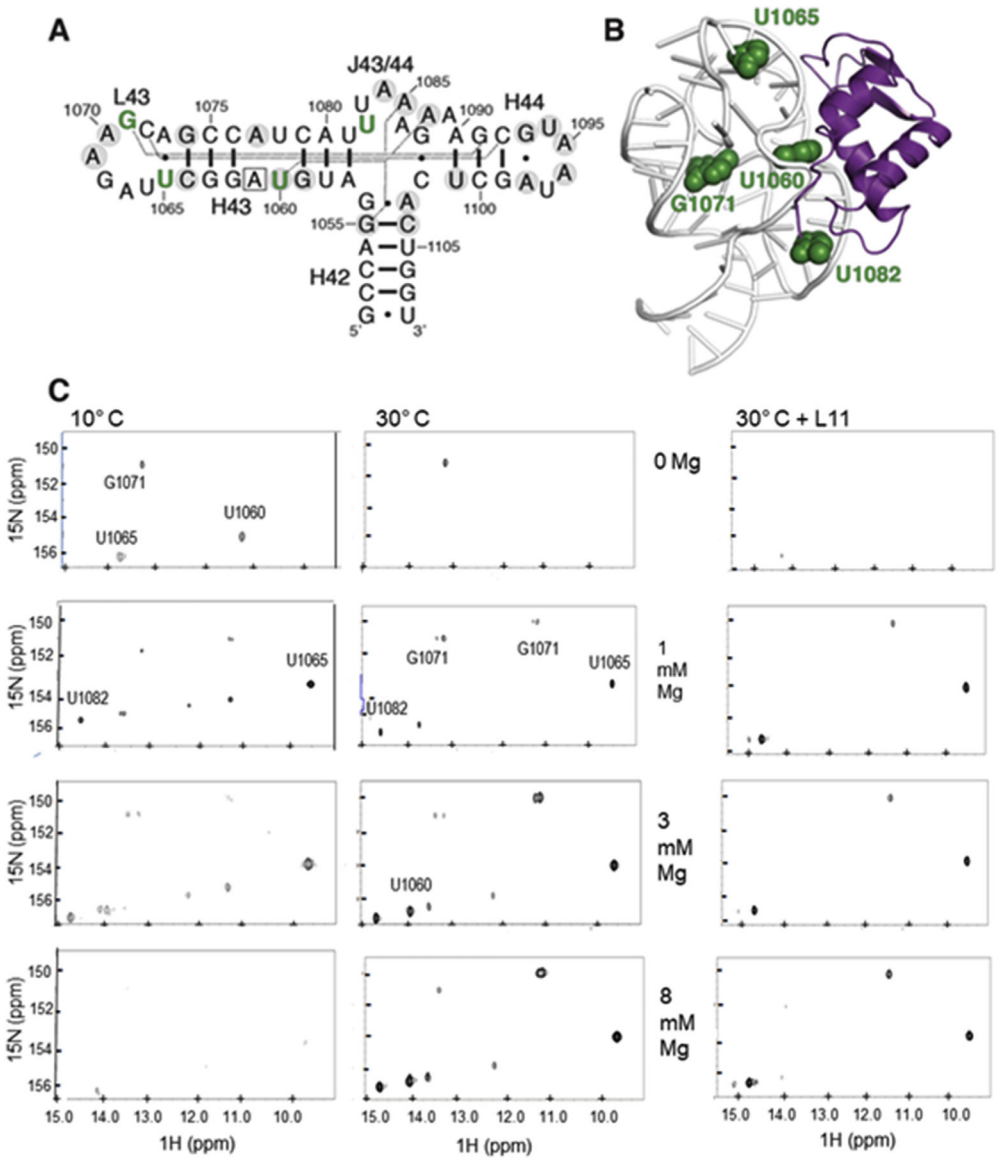

Fig. 7. Imino protons report on formation of GAC tertiary fold with and without L11 CTD.

A. Position of the ^{15}N-labeled nucleotides (green) in **A**. GAC secondary structure and **B**. The cocrystal structure (**PDB ID 1HC8**). C. Imino proton spectra of RNA alone and in the presence of L11 CTD. When L11 CTD is present, addition of Mg^{2+} leads to appearance of only four peaks, which we assign to the canonical tertiary structure. ^{15}N-^{1}H SO-FAST HMQC spectra in 100 mM KCl, 10 mM sodium cacodylate, pH 6.5, [GAC] = 500 μM, and [GAC] = 300 μM, [L11] = 600 μM. 90% H_2O, 10% D_2O, 500 MHz.

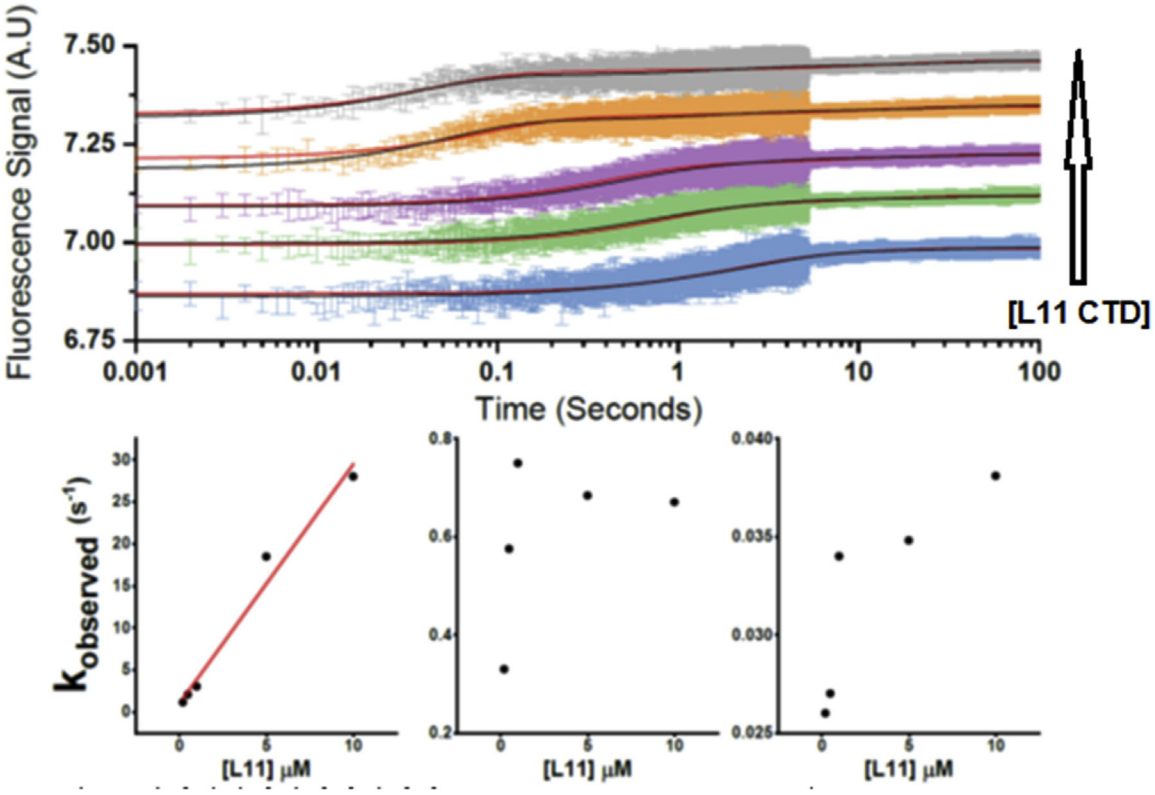

Fig. 8. Kinetics of *Bst* L11 CTD binding to folded A1070AP GAC RNA.

Stopped-flow fluorescence measured by mixing 100 nM A1070AP GAC RNA with L11 protein, at concentrations from 200 nM to 10 mM (arrow). Data (colored traces) are plotted with fits to a three exponential functions (black line). Data are also fit with our genetic algorithm (red line). Each trace is the smoothed average of five replicates. The resulting k_{obs} are plotted against L11 concentration below in the lower panels for $k_{1,obs}$, $k_{2,obs}$, and $k_{3,obs}$, from left to right.

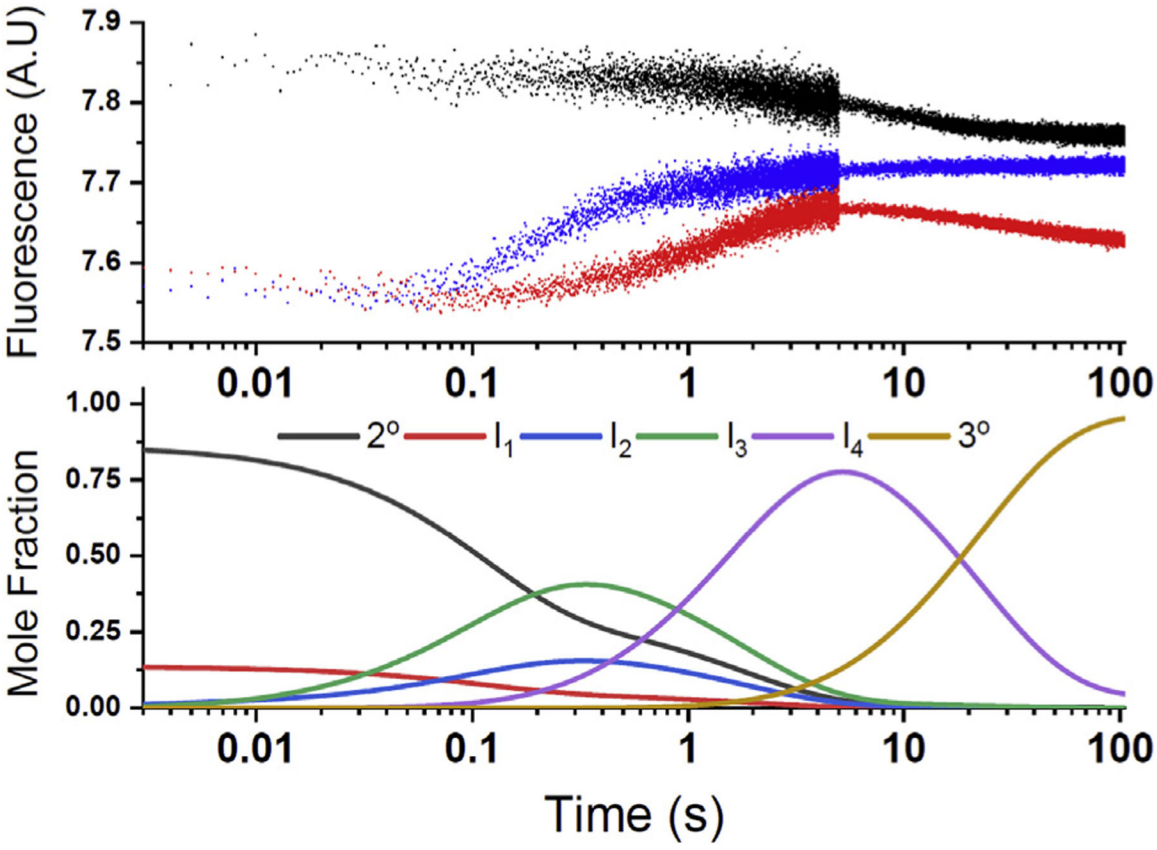

Fig. 9. Coupled A1070AP GAC RNA folding and *Bst* L11 CTD binding.

A comparison of the kinetics of Mg^{2+} association and L11 CTD binding reveals how these two ligands act to influence tertiary folding of the GAC RNA. Top: Red: GAC + 3 mM $MgCl_2$. Black: GAC + 16 μM L11, no Mg^{2+}. Blue: RNA + 30 μM L11 + 3 mM $MgCl_2$ [RNA] = 100 nM. 20 °C. 100 mM KCl, 10 mM sodium cacodylate, pH 6.5. Bottom: Calculation of populations of kinetic intermediates in the kinetic folding scheme.

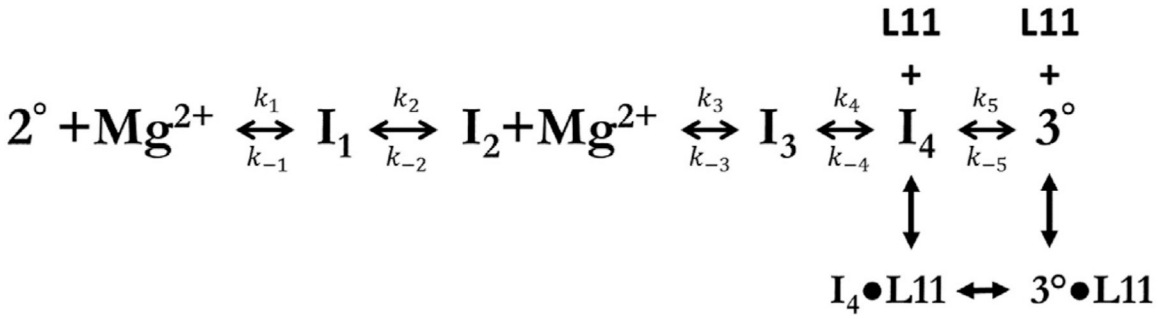

Fig. 10. Schematic of coupled GAC RNA folding and L11 binding pathway.

The change in fluorescence signal in the presence of L11 CTD is coincident with the formation of the intermediate I_4 suggesting that it is the first binding competent intermediate. I_4 is a tertiary structure, but differs from the final fully folded structure (3°).

Table 1.

GAC RNA X-ray data collection, processing, and structure refinement statistics.

	GAC RNA
PDB ID	6PRV
Space group	C2
Resolution (Å)	40–2.7
Cell dimensions	
a, *b*, c (Å)	89.8, 73.6, 130.7
α, β, γ ()	90. 101.1, 90.0
Wavelength	0.9762
R_{meas} [b]	0.086 (2.31)[a]
$CC_{1/2}$	99.9 (48.8)
$I/\sigma I$	12.9 (0.74)
Completeness (%)	97.9 (93.7)
Redundancy	5.1 (4.9)
Unique reflections	22,407
R_{work}/R_{free} [c]	20.4/26.0
Number of atoms	
Protein	5000
Ions	25
Water	2
B-factors	
RNA	108.5
Ion/water	105.5
R.m.s. deviations	
Bond lengths (Å)	0.005
Bond angles ()	1.141

[a] Values in parenthesis are for the highest resolution shell.

[b] $R\text{meas} = \Sigma hkl\, \Sigma i\, |Ii\,(hkl) - \langle I(hkl)\rangle| / \Sigma hkl\, \Sigma i\, Ii(hkl)$.

[c] Rwork = Σhkl| Fo (hkl) - Fc (hkl)| /Σhkl| Fo (hkl), where Fo and Fc are observed and calculated structure factors, respectively. Rfree applies to the 5% of reflections chosen at random to constitute the test set.